Exp Astron
DOI 10.1007/s10686-012-9294-1

ORIGINAL ARTICLE

Achieving sub electron noise in CCD systems by means of digital filtering techniques that lower 1/f pixel correlated noise

Gustavo Indalecio Cancelo · Juan Cruz Estrada · Guillermo Fernandez Moroni · Ken Treptow · Ted Zmuda · H. Thomas Diehl

Received: 14 September 2011 / Accepted: 20 February 2012

Abstract Scientific CCDs designed in thick high resistivity silicon (Si) are excellent detectors for astronomy, high energy and nuclear physics, and instrumentation. Many applications can benefit from CCDs ultra low noise readout systems. The present work shows how sub electron noise CCD images can be achieved using digital signal processing techniques. These techniques allow 0.4 electrons of noise at readout bandwidths of up to 10 Kpixels per second while keeping the full CCD spatial resolution and signal dynamic range.

Keywords CCD · Spectroscopy · Dark matter · Sub electron noise

FERMILAB-PUB-11-391, Work supported by Fermi Research Alliance, LLC under Contract No. DE-AC02-07CH11359 with the United States Department of Energy.

G. I. Cancelo (✉) · J. C. Estrada · K. Treptow · T. Zmuda · H. T. Diehl
Fermi National Accelerator Laboratory, Kirk Road and Pine Street, Batavia, Il 60510, USA
e-mail: cancelo@fnal.gov

J. C. Estrada
e-mail: estrada@fnal.gov

K. Treptow
e-mail: treptow@fnal.gov

T. Zmuda
e-mail: zmuda@fnal.gov

H. T. Diehl
e-mail: diehl@fnal.gov

G. F. Moroni
Instituto de Investigaciones en Ing. Eléctrica (IIIE) "Alfredo C. Desages",
Departamento de Ingenieria Eléctrica, Universidad Nacional del Sur,
Av. Alem 1253 - (B8000CPB), Bahıa Blanca, Argentina
e-mail: fmoroni.guillermo@gmail.com

Published online: 11 April 2012

1 Introduction

CCDs were invented in 1969 [2, 5, 17] and today, after 4 decades of advances in R&D, they have become the sensor of choice for a large number of current and future ground and space telescopes [7, 11, 13]. Scientific CCDs are developed with high performance characteristics such as high quantum efficiencies above 90% in the visible and near-infrared spectrum, large photon dynamic range exceeding 100,000 e^- and pixel size around 10 μm. In particular, the current paper has made extensive use of data acquired with CCDs designed at Lawrence Berkeley National Laboratory (LBNL) [12] and fabricated by Teledyne-DALSA [8]. The CCDs used in our experiments have the characteristics of being thick (e.g. 250 to 600 μm) and developed in high resistivity Si (e.g. 10 kOhm/cm). The high resistivity improves quantum efficiency in the near-infrared up to 1000 nm. The large thickness makes these CCDs massive; hence, excellent detectors for a number of high energy and nuclear physics applications. Just to mention one example, the DAMIC experiment (Dark Matter In CCDs) at the Fermilab National Accelerator Laboratory searches for Dark Matter by measuring the nuclear recoil energy of Weak Interacting Massive Particles (WIMPs) with the Si atom nuclei [10]. A sub electron noise CCD readout system allows sensitivities in the few eV region, which makes DAMIC the most sensitive detector for low mass WIMP search. Sub electron noise CCD readout systems are also important in the design of a new generation of medium resolution optical spectrometers [1, 4]. The sensitivity of medium and high resolution spectrographs can be limited by the readout noise, putting a premium on low-readout-noise systems. Note that in a spectrograph, where the signal can be discriminated from background sky emission lines, an improvement in signal-to-noise accomplished through noise reduction is equivalent to a corresponding increase in the signal accomplished through increasing the area of the primary collecting surface [6, 15].

The remainder of this paper is organized as follows. Section 2 introduces the CCD signal and noise problem. Section 3 shows how the elimination of correlated noise places a lower bound on CCD readout noise. Section 4 describes a new technique to lower the correlated noise. Section 5 shows the achieved sub electron noise results. Section 6 describes the uncertainties of the method and Section 7 shows the hardware implementation of a complete system.

2 CCD signal, architecture and readout

CCDs are organized in one or more arrays of pixels. When properly biased, CCD pixels store charge in a potential well. There are several ways charge can be generated [14, 16] and once collected, the charge can be readout by sequentially shifting it along the CCD vertical columns into an horizontal serial register which is clocked out through an amplifier one pixel at a time. It is common to call the continuous voltage generated by serially clocking

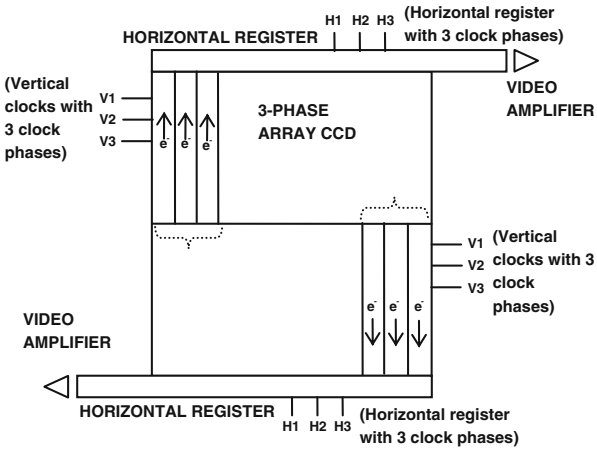

Fig. 1 CCD array showing 2 sets of video channels, and 3-phase vertical and horizontal clocks

pixel charge and pedestals, the video signal. Some CCDs have multiple video outputs which allow splitting the array in blocks and reading them in parallel (Fig. 1).

The CCD transfer function is defined as the inverse of the product of the analog and digital block gains represented in Fig. 2. The total gain is then specified in electrons per digital units of the A/D converter output (e−/ADUs). At high signal levels the noise is dominated by photon statistics and pixel layout non-uniformities. At very low signal levels the noise is dominated by the readout electronics.

When the CCDs are cooled with liquid nitrogen at temperatures of about 173°K the dark current is generally negligible. Furthermore, the charge transfer efficiency (CTE) from pixel to pixel is better than 99.9998% with a total noise contribution of about 0.1%. Hence, the main noise contributors to the CCD data are the internal MOSFET video amplifier and the external readout system.

The CCD output stage generates a video signal as shown in Fig. 3. A reset pulse sets a reference level before a pixel charge is transferred to the sense node capacitor via the output summing well. The video is sensitive to power supply and output MOSFET noise, in particular to their low frequency content.

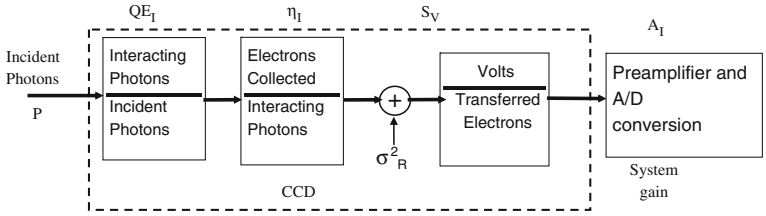

Fig. 2 CCD Block diagram and transfer functions. CCD gain $K = 1/(QEI \cdot \eta_I \cdot S_V \cdot A_I)$

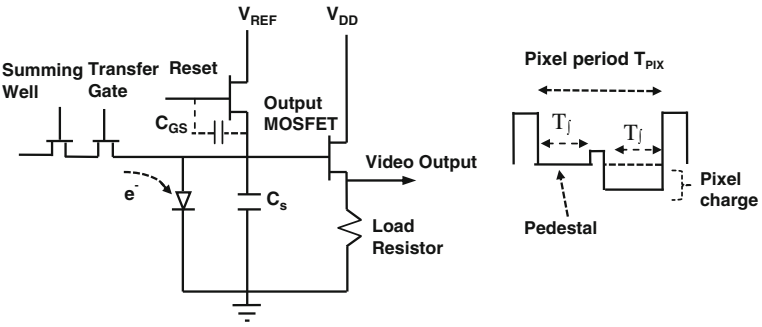

Fig. 3 CCD output amplifier region showing the pixel charge tranfer mechanism via the summing well and transfer gate into the collection node Cs. The Reset clears the charge in Cs after every pixel read out. The right hand side of Fig. 3 shows one pixel video signal including pedestal, pixel and clock feed-throughs

The most common signal readout technique is called Correlated Double Sampling (CDS) which subtracts the average pedestal from the average pixel signal during a predefined time window (1). Figure 4 shows the CDS transfer function as a filter response. CDS is particularly sensitive to low frequency content noise near $0.4/\mathrm{T}_{\int}$. $\mathrm{T}_{\int}$ is the CDS integration time. The CDS differential integral has zeros at frequencies multiple of $\mathrm{T}_{\int}$.

$$s_j^{cds} = \int_{t_{oj}}^{t_{1j}+T_{\int}} p_j + n_{total}(t)dt - \int_{t_{2j}}^{t_{3j}+T_{\int}} s_j + n_{total}(t)dt \tag{1}$$

Where p_j and s_j are the j-th pedestal and pixel respectively, $\mathrm{n_{total}(t)}$ represents the total additive noise (correlated and uncorrelated), and t_{oj}, t_{1j}, t_{2j}, t_{3j} define the limits of the integration windows.

CDS is the optimal filter for a single pixel measurement. However, due to the correlated pink noise, the CDS variance does not monotonically decay towards zero as a function of the integration time ($\mathrm{T}_{\int}$). Pink noise is defined as a noise whose power spectral density decays inversely proportional to the

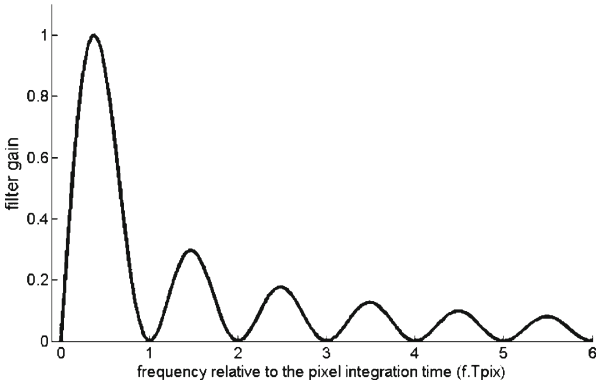

Fig. 4 In frequency domain the CDS integral, (1), can be seen as a filter. Figure 4 shows the CDS transfer function where the frequency axis has been normalized to the pixel readout time Tpix

frequency (i.e. decays as 1/f). Indeed, the noise variance has a minimum at some finite time and then monotonically increases due to the dominant 1/f noise. The minimum noise is achieved close to the frequency where the 1/f noise starts dominating over the White Gaussian Noise. Using DECam CCDs, this frequency has been measured to be between 20 and 25 Kpix/s. [9]. Since the 1/f noise is added by the CCD output amplifiers, we will show in the next sections that the 1/f noise component can be reduced by computing the correlation in a string of neighboring pixels.

3 Pixel correlated noise

Modern CCD readout systems such as the Monsoon for DECam [9] achieve about 2e− R.M.S. of noise at 20 Kpix/s, but the noise rises considerably for slower readouts due to 1/f noise. The same system achieves about 7 e− of noise at 250 Kpix/s meeting the noise specifications for Dark Energy Survey's DECam [11]. Other CDS based systems such as Leach, ESO-FIERA and ESO-NGC share Monsoon's limitation because the 1/f noise correlates among many pixels. The current paper proposes a novel method to lower the CCD system noise to sub electron levels. A new concept is introduced to reduce the correlated noise below what CDS based systems can achieve.

In order to achieve lower noise numbers for the applications mentioned above, it is important to attack the problem in several fronts including: the white Gaussian noise contributions of the upstream sections of the readout system, the EMI contamination due to circuit resonances at high and low frequencies, and the 1/f noise effect on the CDS. The latter is analyzed in Sections 4 to 6 of this paper. The rest of Section 3 describes some of the improvements in the electronics in order to lower the wide band readout noise.

To lower the white Gaussian noise and Electro-Magnetic Interference (EMI) we have designed a special flex cable with balanced video circuits to minimize inductive coupling. Capacitive coupling has also been improved by location and shielding of the video signals. A dV/dt of 250 V/μs produces negligible crosstalk in the video signals.

Power supply noise compensation circuits have been applied to the most sensitive CCD analog powers (i.e. V_{DD} and V_R).

The traditional analog CDS integrator has been replaced by a sampled system. This system employs a so called Σ-Δ 24 bit A to D converter sampling at 20 Ms/s [3]. The A/D includes internal digital filters. We used 2 Finite Impulse Response (FIR) banks as a low pass filter (LPF) with a decimation ratio of 8, setting the Nyquist frequency at 1.25 MHz. The intrinsic noise of the 24 bit A/D system is 1.5 e−/sample and contributes less than 0.25 e− of noise when operated in CDS at 80 kHz (Fig. 5). If the CCD video is pre-amplified by an ultra-low noise amplifier, the A/D noise is further reduced by the pre-amplification gain. In our system a pre-amplification of 4 to 6 is used.

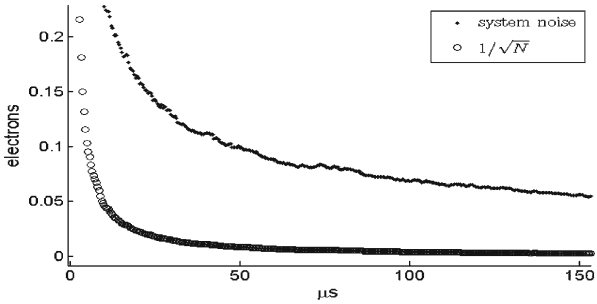

Fig. 5 $\Sigma - \Delta$ 24 bit A/D based readout system noise. Plot vertical axis: RMS noise in electrons; horizontal axis: integration time in μs

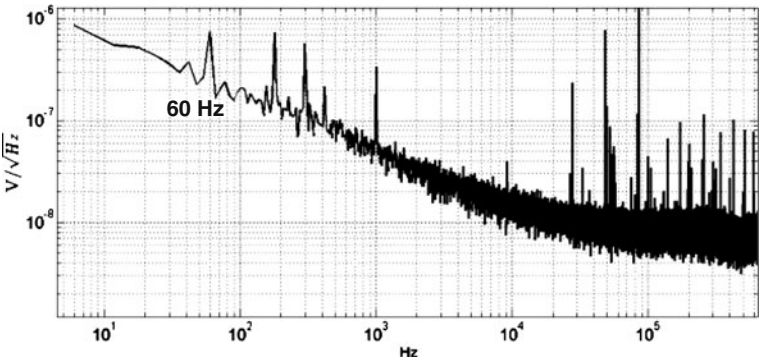

Fig. 6 Readout system noise spectrum. Plot vertical axis: RMS noise in Volts per square root of Hertz; horizontal axis: frequency in Hertz

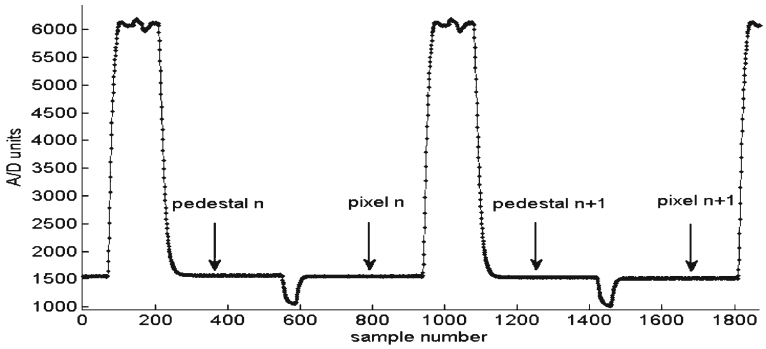

Fig. 7 Video output digitized by the $\Sigma - \Delta$ 24 bit A/D system. The tall signals represent the Reset clock feed-through the stray capacitance C_{GS} (see Fig. 3). The smaller undershoot in between the pedestal and pixel signals are generated by the Summing Well feed-through in a similar manner

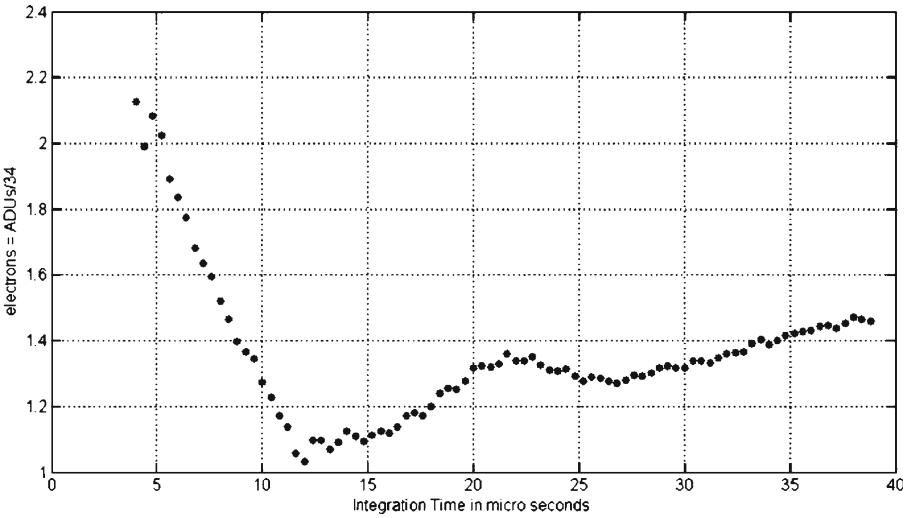

Fig. 8 Digital CDS noise as a function of the CDS integration time. The improvement with respect to the Monsoon system has been achieved improving the EMI, grounding, critical CCD power cleaning, A/D low quantization error and filtering

Figure 6 shows the noise spectrum of the digital readout system. This spectrum shows substantially lower white Gaussian noise than a typical Monsoon system. However, despite efforts in lowering EMI resonances, we can still see 60 Hz and harmonics in the low frequency and other resonances in the higher frequency part. It is worth to mention that the high frequency noise content has a small contribution to the noise when the CCD is readout at low speed.

An example of the video signal sampled by the Σ-Δ 24 bit A/D system is shown in Fig. 7. Since the video data is band limited by an anti-aliasing filter and fast sampled at 20 Ms/s the digital CDS nicely approaches the analog CDS filtering function for the 100 kHz band of interest.

The digital CDS as a function of the pixel integration time $T_{\int}$ is shown in Fig. 8. The system gain has been measured to be 0.025 e−/ADU which shows an increased sensitivity due to the 24 bit ADC. The system's gain has been calibrated using a ^{55}Fe source.

The minimum noise achieved is 1.1 e− at 12 μs of $T_{\int}$. Longer integration times show the effect of the 1/f noise. DES CCDs readout times of 4 μs find noise levels approaching 2.2 e−. The EMI, grounding, critical CCD power cleaning, A/D low quantization error and filtering techniques already result in a factor of 3 in noise reduction with respect to a typical Monsoon system.

4 Estimation of correlated noise

To further reduce system noise the estimation and filtering of low frequency correlated noise content was pursued. The low frequency noise correlates

among many pixels schematically shown in Fig. 9. The following algorithm is used to reduce 1/f or correlated noise:

1) Digitally sample the video signal.
2) Estimate the low frequency correlated (LFC) noise of a string of pixels.
3) Subtract the correlated noise from the original video
4) Perform the digital CDS of the filtered signal.

Step 1) is done by the Σ-Δ 24 bit A/D as described in Section 3. Steps 2) to 4) are done in an FPGA as described in Section 7. Sections 4 to 6 provide fundament to the method; show results and analyze the method errors respectively.

Since the video is sampled the low frequency noise in some number of frequency bands $\Delta f = fs/N$ can be estimated and subtracted. Thus f_s is the sampling frequency and N the number of samples in the data set. For the estimation problem we use a linear χ^2 estimator because it does not assume a particular noise model. χ^2 estimators are not optimal but since the noise spectrum may not be completely Gaussian other estimators cannot claim optimality either. Although the low noise results achieved and shown in Section 5 are very encouraging, the search for a better estimator is not over. The current estimator can be benchmarked using the Cramer-Rao lower bound. There is room for other algorithms to improve the estimation results. However, those studies are not ready yet and will be material for a follow up paper.

N_{pix}, N_s and N are the number of pixels, the number of samples per pixel and the total number of samples used for each correlation analysis.

The signal model is described by

$$x(n) = s(n) + n(n) + w(n) \tag{2}$$

Where s(n) is the noise free video signal composed of pedestals and pixels, n(n) is the correlated noise, and w(n) is the uncorrelated noise.

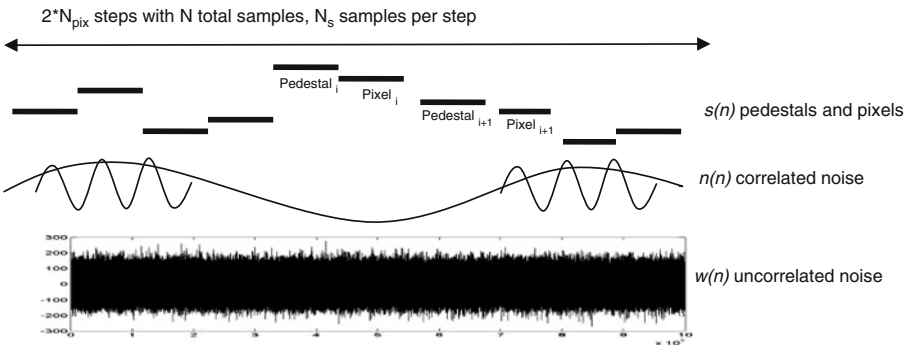

Fig. 9 Signal and noise model showing: s(n) alternated pedestals and pixels, n(n) correlated noise, and w(n) uncorrelated noise

Since pedestal and pixel values are valid during a step function of uniform time we define that as:

$$U_i(n) = U\left(n - iN_{pix}\right) - U\left(n - (i-1)\,N_{pix}\right)$$

Where $U(n - n_0)$ is the Heaviside function centered at time n_0.

The noise free signal can be represented by:

$$s(n) = \sum\nolimits_{i=1}^{2N_{pix}} s_i U_i(n) \tag{3}$$

In (3) s_i alternatively indexes over pedestal i and pixel i from $i = 1$ to $2N_{pix}$.

For the correlated noise we use a Fourier base representation limited to the number of frequency modes M to be estimated:

$$n(n) = \sum\nolimits_{k=1}^{M} c_k e^{2\pi f_k n} = \sum\nolimits_{k=1}^{M} a_k \cos 2\pi f_k n + b_k \sin 2\pi f_k n$$

The number of parameters we need to estimate equals p pixels, p pedestals, and M complex frequencies or 2 M real frequencies (i.e. 2p+2M total). In order to reduce the number of parameters and to improve the estimator covariance we instead use the following input signal

$$y(n) = x(n) - \langle x(n)\rangle_{U_i} \tag{4}$$

Where $\langle x(n)\rangle_{U_i}$ is the average of the signal inside each step $U_i(n)$. Hence,

$$y(n) = n(n) - \langle n(n)\rangle_{U_i} + w(n) \tag{5}$$

The correlated noise averaged in each pixel is expressed by:

$$\langle n(n)\rangle_{U_i} = \sum\nolimits_{i=1}^{2N_{pix}} \left[\left(\frac{1}{N_s}\sum\nolimits_{n\in U_i} n(n)\right) U_i(n)\right] \tag{6}$$

We see that (6) is independent of the true pedestal and pixel values, which are accounted for separately.

The estimator model becomes:

$$y = H.\theta + w \tag{7}$$

where y is N×1 dimensional, θ is the 2 M dimensional parameter vector and H is an N×2M matrix. The H matrix is generated by H = F − E where F is a Fourier base of sines and cosines and E is a matrix of step functions whose values equal to the average of Fourier modes in each pixel interval. As a consequence H is not orthogonal. The parameter estimation is obtained by

$$\hat{\theta} = \left(H^T H\right)^{-1} H^T y \tag{8}$$

Although H is a long matrix in the N dimension the pseudoinverse has to be computed only once.

The estimation process is bounded by computing resources and numerical problems related to matrix size. We have obtained excellent results using discrete data sets of 20 pixels and 20 pedestals. Each data set is a new set of 20 pixels (and pedestals). The system stores no memory from previous

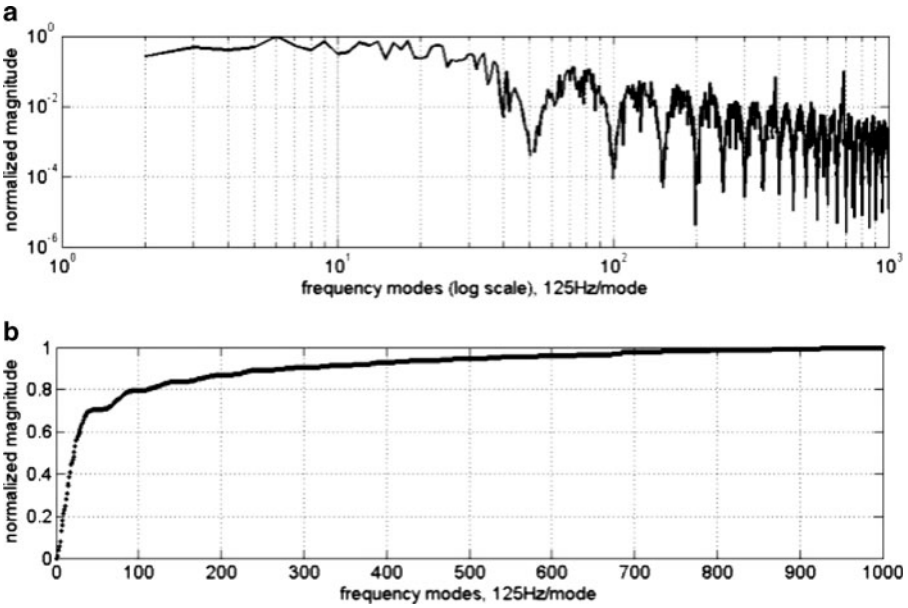

Fig. 10 **a** Noise spectrum weighted by the CDS transfer function. **b** Cumulative correlated noise as a function of the number of modes

estimations. A system with memory (e.g. sequential χ^2 estimator or sliding window) are under study but not implemented yet.

An important step in the estimation process is to determine the number of modes to be estimated. Since the filtered signal is later digitally integrated by the CDS, the noise components are weighted by the CDS transfer function (Fig. 4). Figure 10a shows a typical spectral analysis of the correlated noise for 20 pixels weighted by the CDS transfer function. Figure 10b shows the cumulative noise versus the number of spectral modes. The first 200 low frequency modes, i.e. a 20 kHz total noise bandwidth, account for 85% of the low frequency noise. It is worth mentioning that these plots do not take into account errors in the estimation process which will be analyzed in Section 6.

5 Estimation results

We have applied the estimation and filtering algorithm described in Section 4 to numerous sets of video data.

Some data sets acquired CCD and readout system noise in the video while the CCD clocks are not operating or are operated in reverse. The CCD operated in reverse give us the lowest noise values. We still get all the video amplifier, power supply noise and clock crosstalk but we do not get any charge noise due to leftover charge in the CCD. We have also applied the same methods to normal CCD readout datasets. Figure 11 shows the RMS noise

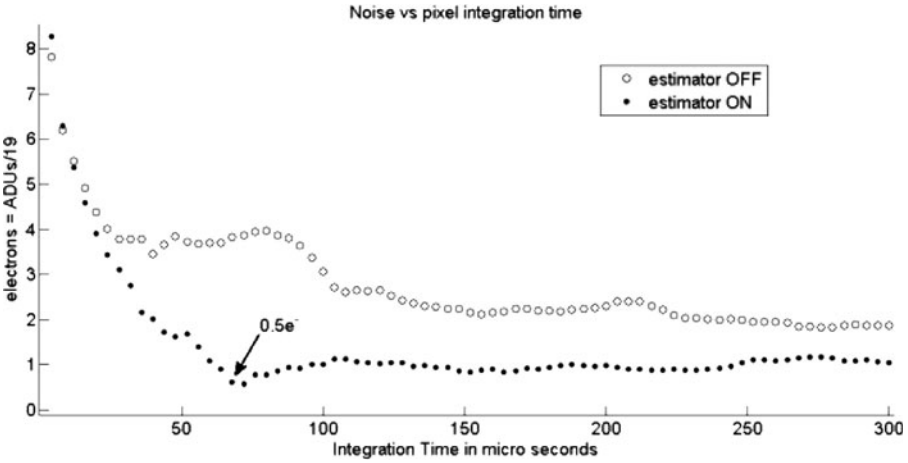

Fig. 11 Comparison of the R.M.S. noise as a function of the CDS integration time for a signal processed by the estimator and the same signal not processed by the estimator

of a 2 channel DES CCD operated normally as a function of the CDS window integration time. The dotted trace video has the correlated low frequency noise cleaned-up by the estimator before computing a digital CDS. For the trace with circles only the digital CDS has been computed. The processed signal achieves a minimum noise of 0.5 e− at about 70 μs. This is an improvement of 3 to 4 over the digital CDS.

The picture in Fig. 12 corresponds to a 12 video channel CCD designed by Berkeley National Laboratory. In this case the video data does not have the CCD clocks running but still measures all the CCD video amplifier noise and system noise, including the 1/f noise. The plot displays the average noise of

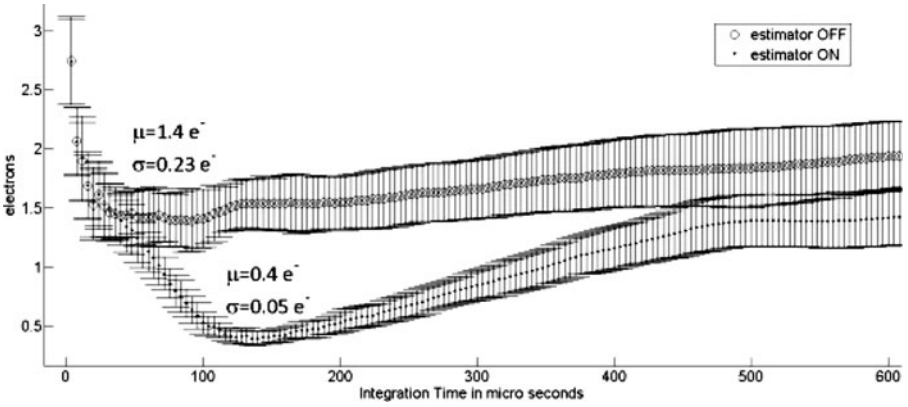

Fig. 12 Comparison of the R.M.S. noise as a function of the CDS integration time for a signal processed by the estimator and the same signal not processed by the estimator. Plot also shows 1-σ error bars

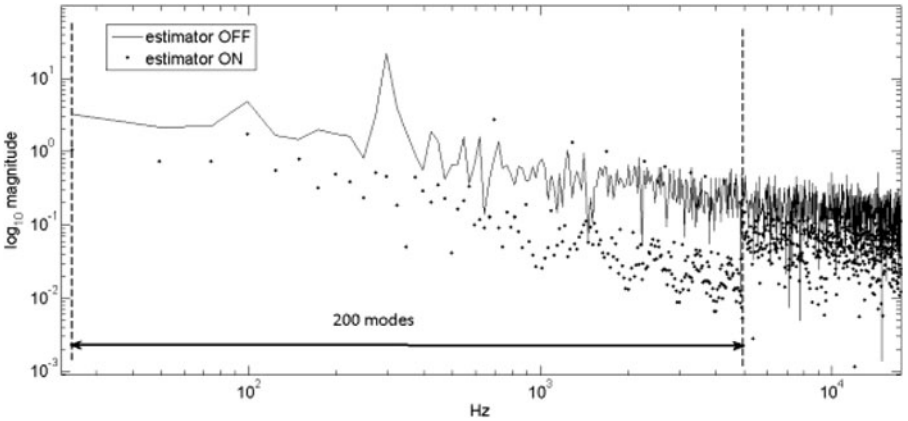

Fig. 13 Noise spectrum comparison between a signal processed by the estimator and the same signal not processed by the estimator

100 data sets and 1-σ error bars. The signal processed by the estimator has a minimum noise of 0.4 e− at 120 μs, which is a factor of 3.5 times better than the digital CDS alone. It is also interesting that the 1-σ error bars of the estimator processed data are 4 times smaller than the ones for the unprocessed data. The plot also shows increasing noise at longer integration times due to residual 1/f noise.

Figure 13 compares the noise power spectrum of the unfiltered signal and the filtered signal after the low frequency estimation of 200 modes has been subtracted. On average, the LFC noise has been reduced by almost an order of magnitude. It can also be observed that the filter works more effectively for the higher estimated modes due to non-uniform estimation errors. Please note that the noise and spectrum plots of Figs. 11, 12 and 13 are affected by estimation errors, which are the main limitation to achieving further noise reduction.

6 Estimation error

The estimation errors can be computed using the χ^2 covariance matrix

$$C_\theta = \left(H^T C_y^{-1} H\right)^{-1} \tag{9}$$

If the uncorrelated noise is WGN$\sim(0,\sigma^2)$ (9) can be expressed by

$$C_\theta = \sigma^2 \left(H^T H\right)^{-1} \tag{10}$$

The error amplification matrix $(H^T H)^{-1}$ in (10) can be computed numerically. Since H is not orthogonal, $(H^T H)^{-1}$ is not diagonal and the θs will be correlated. Also note that each entry in $(H^T H)^{-1}$ is inversely proportional to the number of samples N used in the estimation.

The main problem in the estimation of Low Frequency Correlated noise is that due to the non orthogonality of H, the inverse problem becomes ill-conditioned as we increase the numbers of parameters to be estimated. Figure 14 shows the estimation error is proportional to $(H^TH)^{-1}$ as a function of the number of modes in H for up to 200 modes. Since the errors in θ are directly proportional to $(H^TH)^{-1}$ (i.e. (10)), for a large H small oscillations in the data produce large variations in the parameter vector θ.

The estimator has been analyzed using Singular Value Decomposition (SVD) and generalized SVD techniques for several (H,L) pairs, where L is a linear operator. The minimization procedure was carried using Tikhonov's rule:

$$\min_{\theta} = \left\{ \|H\theta - y\|^2 + \|Ly\|^2 \right\}$$

We also observe that the low frequency estimation errors have a heavier weight. Figure 15 shows the error amplification of $(H^TH)^{-1}$ normalized to N = 1 for a 200 mode estimator versus a 20 mode estimator. The 200 mode estimator has almost an order of magnitude more error in the first 15 modes due to mode correlation.

The low noise results shown in Figs. 11, 12 and 13 have been obtained using a slightly different approach. Instead of inverting a large (i.e. 200 mode matrix) a series of smaller matrices (i.e. 20 modes) are inverted and used for estimation. The reasoning is that LF noise modes that are far away from each other are uncorrelated. This method is effective and keeps the C_θ small for most θ_i. However, as it can be seen in Fig. 13, a few modes have a large estimation error. The optimal solution to minimize the C_θ is still open.

Currently, the white Gaussian noise σ has been improved to 1.8 nV/sqrt(Hz). The total estimation error is numerically computed and shown to be about 0.1 e−.

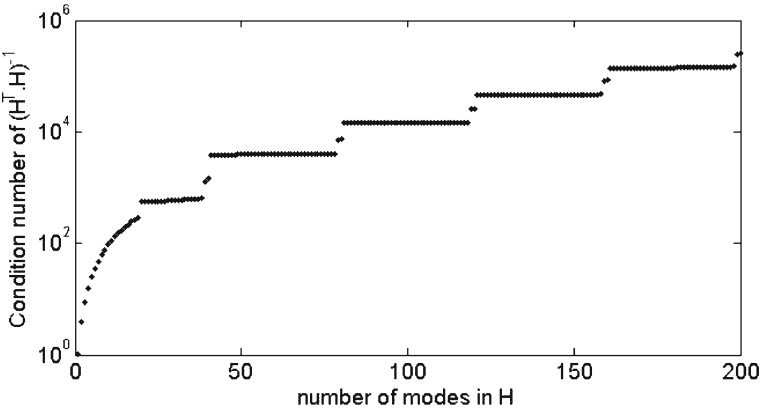

Fig. 14 Estimation error analysis. H^TH condition number as a function of the number of estimated modes

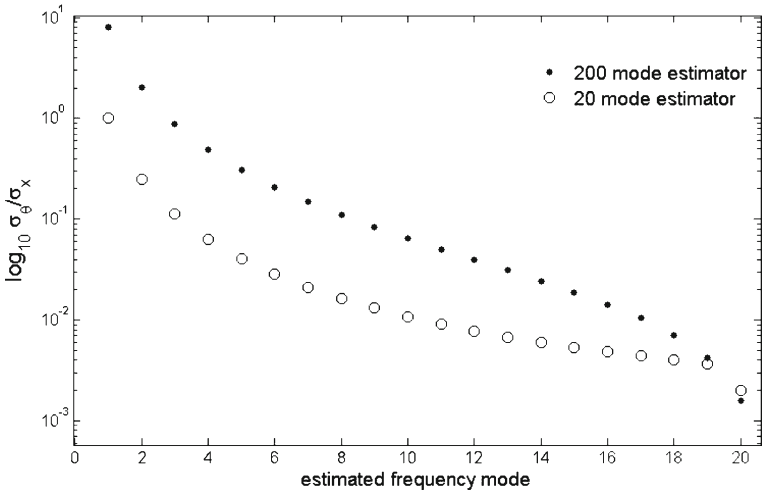

Fig. 15 Estimation error as a function of the estimated mode

7 Hardware implementation

The estimator and digital CDS reduce the CCD noise deep into the sub-electron region. The price to pay for lower noise is a more sophisticated readout system. The estimator requires a Field Programmable Gate Array (FPGA) or processor capable of performing millions of multiplications per second, subtracting the estimated low frequency noise from the original signal and digitally computing the CDS of the filtered signal. However, modern FPGAs have enough horsepower to process and filter several video channels.

The example in this paper estimates correlated noise in data sets of 20 pixels long and shows a minimum for an integration time of about 120 μs (Fig. 12). The data is sampled at 20 MHz and pre-filtered and decimated, producing a data stream of 125 Ksamples/s. Each 20 pixel dataset is 5 ms long and has 6000 samples. The number of multiplications required for the estimation of 2 times 200 modes is 2.4 million in 5 ms or 480 million multiplications/s. The filter reconstruction requires the same number for a total of 960 million multiplications/s. Modern FPGAs have hundreds and even a couple of thousands of multipliers running up to 400 million multiplications/s. It is also worth mentioning that the pseudo inverse of H needs to be computed only once, so it can be computed off line and stored in memory. The memory requirements are N by 2 M, that is 7.2 MB for the current example. The memory requirements to process 20 pixels of sampled data are (i.e. 6000 samples) is 18 KB. This memory area can be overwritten by the next 20 pixels.

Figure 16 shows a fits image taken with the FPGA based digital CDS. This is a 1 K × 4 K image processed following the algorithm described in Section 4. The small with dots are mostly diffusion limited x-rays coming from an ^{50}Fe souce. The x-rays create a narrow histogram peaking at 1620 e^- above the

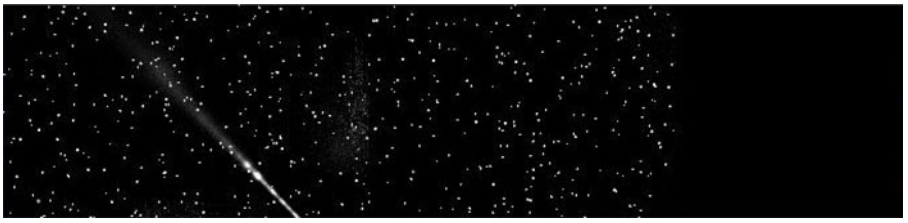

Fig. 16 CCD image taken with the FPGA based digital CDS. The image is 1 K × 4 K pixels showing mostly x-rays coming from an ^{50}Fe souce and a muon track on the lower left. The dark portion on the right is the CCD over-scan

background noise (i.e. dark background in image). We can also see a cosmic muon track on the lower left. The dark portion on the right is the CCD over-scan. The noise of this image is 0.5 e^-.

8 Conclusions and future work

Fast sampling and digital processing the CCD video signal allows us to reduce the low frequency noise that correlates pixel to pixel. Deep sub electron noise of 0.4 e^- and 1-σ error bars of 0.05 e^- have been systematically achieved by this method. The readout bandwidth is about 4 Kpix/s. We have also achieved 1 e^- of noise at 42 Kpix/s by minimizing EMI, crosstalk, and power supply noise. Digital CCD readout systems are more sophisticated than traditional analog CDS and can significantly improve signal to noise ratio.

For spectrometers the benefit is a better signal to noise ratio, which can be used to improve spectrum resolution or to reduce the size of the spectrometer.

For particle detectors the method described improves the sensitivity of detecting very low energy nuclear recoils. Experiments such as Direct Dark Matter search and coherent neutrino scattering produce a low counting rate of recoils amid potentially large backgrounds. These backgrounds, mainly cosmic rays and ionizing radiation, are largely suppressed by several types of shielding. Unfortunately, shielding cannot achieve 100% efficiency. However, the number of nuclear recoils grows exponentially with the detector energy sensitivity. A 0.5 e− noise system allows setting the energy threshold at ∼10 eVee.

A readout speed of 4 Kpix/s is more than enough for low counting rate particle physics experiments. In fact these experiments read the CCDs only few times a day. Furthermore, 1 e− of noise has been achieved for 50 Kpix/s by minimizing noise sources and improving groundings, without the need of using the estimator technique. In order to take advantage of the estimation technique at faster readout speeds the White Gaussian noise density must be reduced with respect to the CCD gain. Presently, this limit is imposed by the CCD video MOSFET that has a noise floor of 5 nV/$\sqrt{\text{Hz}}$ and a gain of 2.5 $\mu V/e^-$. The White Gaussian noise contribution before integration

scales up/down linearly with the square root of the bandwidth. The noise contribution is only partially filtered by the CDS as depicted in Fig. 4. The effectiveness of the CDS is the same for either the analog or fast sampling digital implementation of the CDS algorithm.

The limitation of the correlated noise estimation technique is given by the parameter covariance matrix of (10). There we see that the parameter estimation error is proportional to the variance of the White Gaussian noise and also proportional to $(H^T H)^{-1}$. The last term is inversely proportional to the number of samples used for the estimation. A faster pixel readout, at the same sampling rate, would lower the number of samples available to the χ^2 algorithm increasing the parameter covariance errors and limiting the effectiveness of the estimator technique.

A potential solution to the last problem could be a continuous estimation of the low frequency noise using a sequential χ^2 algorithm, a moving window, or a Kalman filter. These techniques have not been investigated yet and are open to future work.

Acknowledgements We want to thank the Fermilab staff at SiDet facility, in particular Kevin Kuk, Donna Kubik, Walter Stuermer who helped us with the operations of CCDs systems; and Stephen Holland from Lawrence Berkeley National Laboratory for always being available to answer our CCD questions.

References

1. Abdalla, F., et al.: The dark energy spectrometer (DESpec): a multi-fiber spectroscopic upgrade of the dark energy survey and camera for the Blanco Telescope. In preparation
2. Amelio, G.F., Tompsett, M.F., Smith, G.E.: Experimental verification of the charge coupled device concept. Bell Syst. Tech. J. **49**(4), 593–600 (1970)
3. Analog Devices: 2.5 MSPS, 24-Bit, 100 dB Sigma-Delta ADC with On-Chip Buffer, Analog Devices. http://www.analog.com/static/imported-files/data_sheets/AD7760.pdf (2006)
4. Schlegel, D., et al.: BigBOSS: the ground-based stage IV dark energy experiment. http://arxiv.org/abs/0904.0468 (2009)
5. Boyle, W.S.: Nobel lecture: CCD—an extension of man's view. Rev. Mod. Phys. **82**(3), 2305–2306 (2010)
6. Chandler, C.E., Bredthauer, R.A., Janesick, J.R., Westphal, J.A., Gunn, J.E.: Sub-electron noise charge coupled devices. SPIE Charg.-Coupled Devices Solid State Opt. Sens. **1242**, 238–251 (1990)
7. Diehl, H.T., et al.: Characterization of DECam focal plane detectors. In: Dorn, D.A., Holland, D. (eds.) High Energy, Optical and Infrared Detectors for Astronomy III, Proceedings of the SPIE, vol. 7021, p. 70217 (2008)
8. DALSA-Teledyne: http://www.dalsa.com/
9. Estrada, J., et al.: CCD testing and characterization for Dark Energy Survey. In: McLean, I.S., Iye, M. (eds.) Ground-Based and Airborne Instrumentation for Astronomy, Proceedings of the SPIE, vol. 6269, p. 62693K (2006)
10. Estrada, J., et al.: Prospects for a direct dark matter search using high resistivity CCD detectors. arXiv:0802.2872v3 [hep-ex](1Jul2008) (2008)
11. Flaugher, B.: The Dark Energy Survey instrument design. In: McLean, I.S., Iye, M. (eds.) Ground-Based and Airborne Instrumentation for Astronomy, Proceedings of the SPIE, vol. 6269 (2006)

12. Holland, S.E., Groom, D.E., Palaio, N.P., Stover, R.J., Wei, M.: Fully depleted, back-illuminated charge-coupled devices fabricated on high-resistivity silicon. IEEE Trans. Electron Devices **50**(1), 225–238 (2003)
13. Honscheid, K., DePoy, D.L.: The Dark Energy Camera (DECam). A new instrument for the Dark Energy Survey. IEEE Nuclear Science Symposium Conference Record NSS '08, pp. 3357–3360 (2008)
14. Janesick, J.R.: Scientific Charge Coupled Devices. SPIE Publications, Bellingham, Washington (2001)
15. Janesick, J.R., et al.: New advancements in charge-coupled device technology: sub-electron noise and 4096×4096 pixel CCDs. SPIE Charg.-Coupled Devices Solid State Opt. Sens. **1242**, 223–237 (1990)
16. McLean, I.: Electronic Imaging in Astronomy—Detectors and Instrumentation, 2nd edn. Springer-Praxis, Berlin (2008)
17. Smith, G.E.: Nobel lecture: the invention and early history of the CCD. Rev. Mod. Phys. **82**(3), 2307–2312 (2010)
18. Wey, H.M., Guggenbuhl, W.: An improved correlated double sampling circuit for low noise charge coupled devices. IEEE Trans. Circuits Syst. **37**(12), 1559–1565 (1990)